

A Simple Method for the Synthesis of $KV_3O_8 \cdot 0.42H_2O$ Nanorod and Its Lithium Insertion/Deinsertion Properties

Bijun Feng, Dan Sun, Haiyan Wang*, Shuai Tan, Hui Zhang

Key Laboratory of Resources Chemistry of Nonferrous Metals, Ministry of Education, School of Chemistry and Chemical Engineering, Central South University, Changsha, 410083, P.R China

*E-mail: wanghy419@126.com

Received: 18 November 2012 / Accepted: 13 December 2012 / Published: 1 January 2013

A facile and large-scale hydrothermal method was introduced to synthesize KV_3O_8 nanorod as cathode material for Li-ion battery. The nanorods are composed of $KV_3O_8 \cdot 0.42H_2O$ based on the results of X-ray diffraction (XRD), Fourier transform infrared spectrum (FT-IR), differential scanning calorimetry and thermal gravimetry (DSC/TG). Meanwhile, it shows a width of 80-230 nm and a length of up to several micrometers by transmission electron microscopy (TEM). The nanorods deliver an initial specific discharge capacity of 130.1 mAh g^{-1} during 1.5~4.0 V at 15 mA g^{-1} , with a capacity retention of 87.9% after 20 cycles. XRD results confirm that the electrode possesses good structure stability during lithium ion insertion and extraction.

Keywords: Li-ion battery; KV_3O_8 nanorod; Hydrothermal approach; Electrochemical performance

1. INTRODUCTION

One-dimensional (1D) nanostructured materials have attracted considerable attention for advanced functional systems owing to their attractive properties [1]. During the past decade, research has focused on nanostructured electrode materials for Li-ion battery to improve electrochemical performance [2-6]. It is well known that 1D nanostructured electrode materials possess the high surface-to-volume ratio and excellent surface activities, which have stimulated great interest in their development for the next generation of power sources [3,4]. Among the various preparation methods, hydrothermal method is considered to be the most promising one for nanostructured electrode material [6].

Nanostructured vanadium oxides and their derivative compounds have been widely proposed as cathode materials for Li-ion battery due to high capacity and low cost [7-12]. Much interest centres on lithium trivanadate (LiV_3O_8), the most prominent member of this family [9,10]. However, electrochemical performance of LiV_3O_8 is highly dependent on preparation methods that influence its morphology, particle size and crystallinity [11]. In addition, to the best of our knowledge, LiV_3O_8 could not be obtained by one-step hydrothermal method. In our recent work, we introduced a new cathode material ammonium trivanadate by one-step and facile hydrothermal reaction, which showed a maximum discharge capacity of 225.9 mAh g^{-1} with good cycling stability [13]. It was found that both Li^+ in LiV_3O_8 and NH_4^+ group in $\text{NH}_4\text{V}_3\text{O}_8$ could not be extracted from the host materials and probably acted as pillar to stabilize the crystal structure [10,13], which inspires us to use other cations, such as Na^+ or K^+ to replace Li^+ or NH_4^+ to form new cathode materials for Li-ion battery [14,15].

Potassium trivanadate compounds have been prepared by several synthesis methods [15-17]. However, no 1D nanostructured KV_3O_8 was reported. KV_3O_8 was hydrothermally grown at $250 \text{ }^\circ\text{C}$ from V_2O_5 powder dispersed in KNO_3 solution [15]. West et al. [16] fabricated KV_3O_8 with high initial discharge capacity for Li-ion battery by a solution approach. However, no cycling performance was shown in their work. Menav et al. [17] employed a high temperature solid-state reaction to prepare KV_3O_8 . The electrode exhibited only an initial discharge capacity of less than 100 mAh g^{-1} and poor cycling performance. Much more work should be done for this kind of material. In current work, we propose a facile and large-scale preparation method to synthesize 1D KV_3O_8 nanorods using V_2O_5 and KOH as raw materials. Its lithium insertion/deinsertion properties are also investigated in details.

2. EXPERIMENTAL

2.1 Synthesis and characterization of KV_3O_8

The starting materials, V_2O_5 and potassium hydroxide were of analytical purity and directly used without any purification. At first, 0.909 g V_2O_5 and 0.281 g KOH were dissolved in deionized water successively. After gentle heating and proper stirring for 0.5 h , the mixed solution was then transferred to 50 ml Teflon lined stainless steel autoclave. The total volume of the solution was about 40 ml . The autoclave was sealed and heated at $180 \text{ }^\circ\text{C}$ for 48 h and then cooled to room temperature naturally. The obtained precipitates were filtered, washed with deionized water three times. Finally, the precipitates were dried at $80 \text{ }^\circ\text{C}$ overnight to obtain the KV_3O_8 powder.

All X-ray diffraction (XRD) data were given by a Philips X-Pert system (Cu-K α radiation) with a step of 0.02 ° . Fourier transform infrared (FT-IR) spectra were recorded using the Nicolet 6700 FT-IR spectrometer. Differential scanning calorimetry and thermal gravimetry (DSC/TG) was carried out with a NETZSCH STA 449C differential scanning calorimeter under N_2 atmosphere at a ramping rate of $10 \text{ }^\circ\text{C min}^{-1}$. Morphological studies were conducted using a JEOL JEM-2011 transmission electron microscopy (TEM).

2.2 Electrochemical measurements

The electrochemical cells were constructed by mixing the active material, polytetrafluoroethylene (PTFE), and carbon black in the weight ratio of 80:10:10. The slurry was cast onto Al foil. After well-drying, the electrodes were assembled into CR2016 coin-type cells with commercial electrolyte (Merck; 1 M LiPF₆ in 1:1 v/v ethylene carbonate/dimethyl carbonate) and a Li metal as counter electrode. The cells were constructed in an Ar-filled MBraun glovebox and cycled galvanostatically between 1.5 and 4.0 V (voltage unit in this paper is versus Li/Li⁺) at a desired current density with a Land CT2001A tester system at room temperature. Cyclic voltammetry (CV) test was carried out using the electrochemical station (Shanghai Chenhua, China) with a scan rate of 0.1 mV s⁻¹ at room temperature.

3. RESULTS AND DISCUSSION

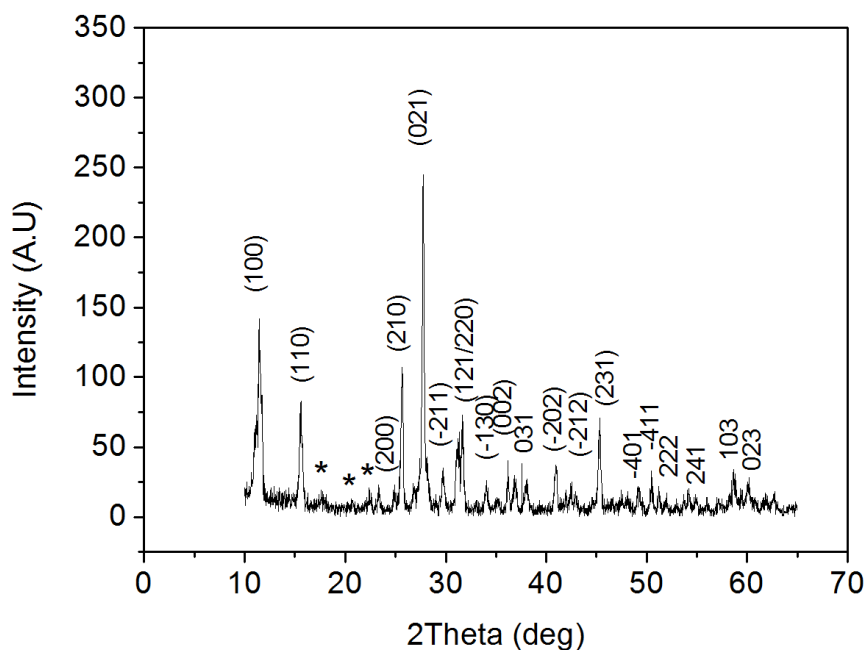


Figure 1. XRD pattern of as-prepared powder.

XRD pattern of as-prepared powder is shown in Fig. 1. The diffraction peaks can be easily indexed into KV₃O₈ with monoclinic structure and P2₁/m space group (JCPDS card No.22-1247) [16,17]. Meantime, several unidentified impurity peaks with tiny intensity at 17.5°, 20.7° and 22.5° are also observed. The obtained lattice parameters are $a = 0.8016$ nm, $b = 0.8085$ nm, $c = 0.5339$ nm and $\beta = 98.17^\circ$, which are a little different from the values of JCPDS card No.22-1247 ($a = 0.7644$ nm, $b = 0.8395$ nm, $c = 0.4980$ nm and $\beta = 96.98^\circ$). The as-prepared KV₃O₈ indicates a little larger unit cell volume (0.3425 nm³) than that (0.3172 nm³) of above standard card. Such differences are probably due to the certain amount of crystal water in KV₃O₈ host, as that in NH₄V₃O₈·0.2H₂O [13], which is further verified by the following FT-IR and DSC/TG results. Analysis of the largest diffraction peak (021)

using the Scherer formula reveals grain sizes of 33.1 nm. Apparently, the crystal structure of as-prepared KV_3O_8 is different from those of LiV_3O_8 [10], $\text{NH}_4\text{V}_3\text{O}_8$ [13,18] and NaV_3O_8 [19], which probably means different electrochemical performance.

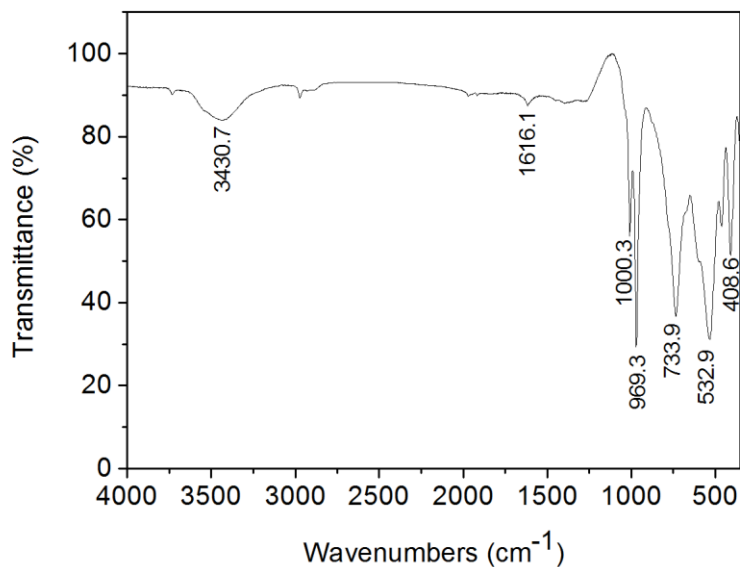


Figure 2. FT-IR spectrum of as-prepared powder.

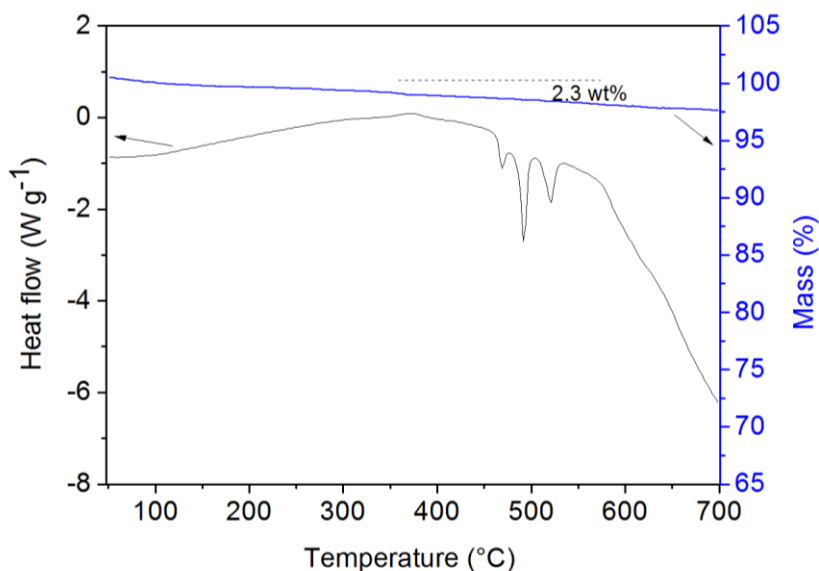


Figure 3. DSC/TG curve of as-prepared KV_3O_8 powder.

Fig. 2 depicts FT-IR spectrum of as-prepared KV_3O_8 powder. As can be seen, the sample indicates the bands at about 3430.7, 1616.1, 1000.3, 969.3, 733.9 and 532.9 cm^{-1} , respectively. The bands at 1000.3 and 969.3 cm^{-1} are due to $\text{V}=\text{O}$ stretching of distorted octahedral and distorted squarepyramids, while those at 733.9 and 532.9 cm^{-1} can be assigned to asymmetric and symmetric

stretching vibration of V-O-V bonds [13, 20]. Moreover, the two weak bands at 3430.7 and 1616.1 cm^{-1} in the spectrum can be assigned to the O-H stretching vibrations and H-O-H bending motion [21], respectively, suggesting the as-obtained material contains certain crystal water. DSC/TG curve (Fig. 3) was investigated to make sure the amount of crystal water in KV_3O_8 . From the weight loss (2.3%) of the sample between 100 and 600 $^\circ\text{C}$, it is deduced that the amount of crystal water is about 0.42 per unit. Thus, results above demonstrate that the as-prepared material is actually composed of $\text{KV}_3\text{O}_8 \cdot 0.42\text{H}_2\text{O}$.

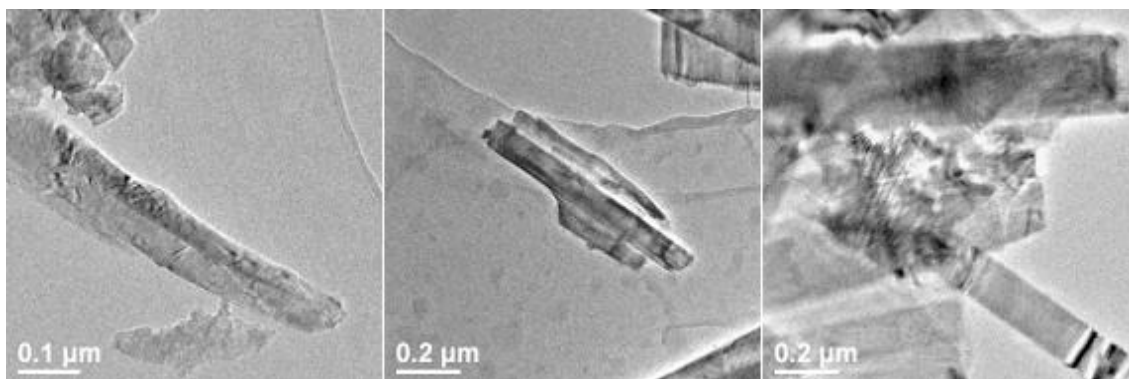


Figure 4. TEM images of KV_3O_8 powder.

As displayed by the different magnification TEM images of KV_3O_8 powder (Fig. 4), this material shows rod-like morphology with 80 - 230 nm width and several micrometers length. It's noted that some of primary nanorods are partially attached together to form large one. It also should be pointed out that a few defects or dislocations are observed on some nanorods.

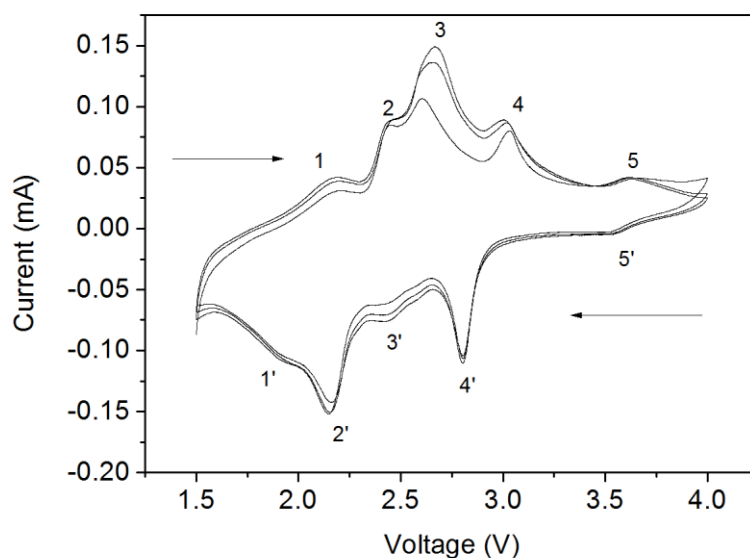


Figure 5. Cyclic voltammety curves of KV_3O_8 electrode between 1.5 and 4.0 V at scanning rate 0.1 mV s^{-1} .

Fig. 5 shows CV curves of KV_3O_8 electrode between 1.5 and 4.0 V at scanning rate 0.1 mV s^{-1} . Two obvious pairs of redox peaks, with the oxidation peaks located at about 2.61 V, 3.03 V and the corresponding reduction peaks at about 2.14 V, 2.80 V, respectively, are observed. Besides, there are also two tiny pairs of redox peaks, showing the oxidation peaks at about 2.17 V, 3.62 V and the corresponding reduction peaks at about 1.94 V, 3.57 V, respectively. Appearance of redox peaks indicates the reversible Li^+ de-intercalation and intercalation in solid phase [22-25], suggesting the multi-steps electrochemical processes of KV_3O_8 . It should be noted that there is only a little peak area loss in CV reduction curves during the first three cycles, which is in good agreement with the cycling stability shown in Fig. 6.

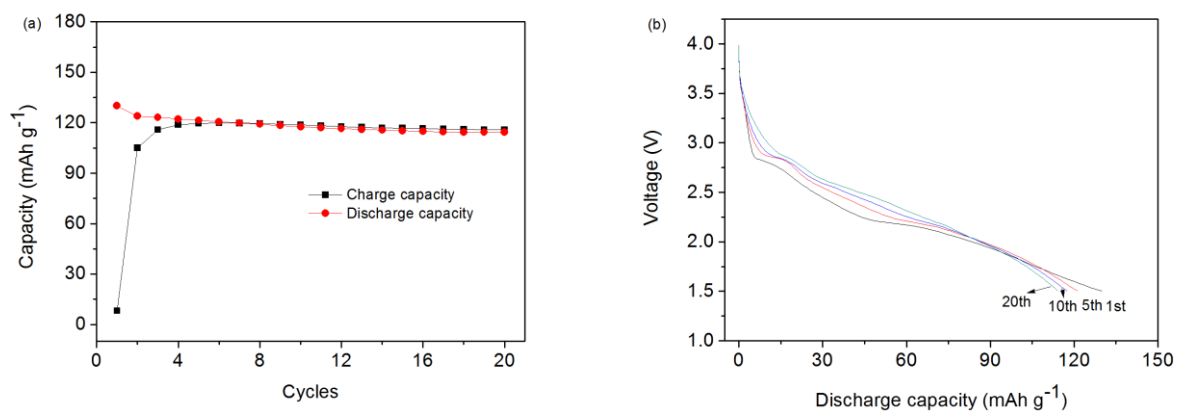


Figure 6. Cycling performance (a) and discharge curves at different cycle of KV_3O_8 operated between 1.5 and 4.0 V at a current density of 15 mA g^{-1} .

The specific charge-discharge capacities versus cycle numbers of KV_3O_8 electrodes at a current density of 15 mA g^{-1} between 1.5 and 4.0 V is displayed in Fig. 6(a). Fig. 6(b) shows the discharge curves at the 1st, 5th, 10th and 20th cycles. The KV_3O_8 nanorods deliver an initial specific discharge capacity of 130.1 mAh g^{-1} (about 1.554 electrons per unit formula are exchanged), which is less than those of LiV_3O_8 [10], $\text{NH}_4\text{V}_3\text{O}_8$ [13] and NaV_3O_8 [19]. However, it is higher than that in literature by solid state method [17], due to the nanorod morphology [4]. As shown in Fig. 1, KV_3O_8 possesses different crystal structure from the other three alkali-metal trivanadates [16], in which there are less available reversible lithium ion sites. $\text{KV}_3\text{O}_8 \cdot 0.42\text{H}_2\text{O}$ consists of V_3O_8 layers and interstitial hydrated K ions. The V_3O_8 layer is composed of corrugated sheets of distorted, edge sharing VO_6 octahedra and the hydrated K ions are located between the layers [16]. It is probable that the large K ions could hinder some pathways for lithium ion transferring. The discharge capacity retains 114.3 mAh g^{-1} at the 20th cycle, about 87.9% of the initial capacity. It is worthwhile to note that obvious capacity loss occurs in the first several cycles and then the discharge capacity keeps more stable, which are consistent with the discharge curves in Fig.6 (b). The capacity loss in the first several cycles should be attributed to the large polarization of electrode and probable slight structure rearrangement due to lithium ion insertion, as that of $(\text{NH}_4)_{0.5}\text{V}_2\text{O}_5$ [23]. Apart from the first several cycles, the KV_3O_8 nanorod indicates good cycling stability. In addition, it can be seen that the initial charge capacity is

only 8.1 mAh g^{-1} , close to zero, which is in good accordance with other alkali-metal trivanadates [10,13,19].

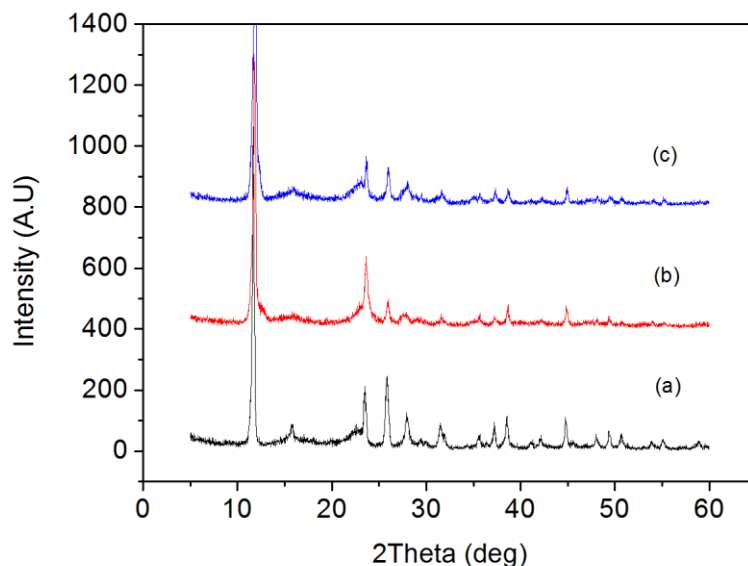


Figure 7. XRD patterns of KV_3O_8 electrodes at different voltages after cycling: (a) no cycling; (b) discharge to 1.5 V at the 1st cycle; (c) charge to 4.0 V at the 2nd cycle.

XRD patterns (Fig. 7) of KV_3O_8 nanorods at different voltages after cycling were also investigated to further understand the charge-discharge mechanism. The electrode consisting of active material, carbon and binder, after washing with DMC and dried for 2 h, was directly used to examine the structure. As shown, the electrode a shows the similar XRD patterns with KV_3O_8 powder in Fig. 1, except intensity changes in some diffraction peaks. Such phenomenon was also demonstrated in our previous work [23] and should be attributed to the smoother surface of electrode film in comparison with the powder. After the electrode is discharged to 1.5 V, the diffraction peaks (100), (210), (021) and (231) shift toward large angle direction while (-211) move toward opposite direction. In addition, the diffraction intensity of peaks (110), (021) and (-211) decrease with lithium ion insertion into KV_3O_8 host and then increase again when charging to 4.0 V. It can be seen that sample a, b and c indicate very similar XRD patterns, implying that KV_3O_8 electrode possesses good structure stability and no new phase appears during lithium ion insertion and extraction.

4 .CONCLUSIONS

In summary, $\text{KV}_3\text{O}_8 \cdot 0.42\text{H}_2\text{O}$ nanorod with a width of 80-230 nm and a length of several micrometers was synthesized by a facile hydrothermal method as cathode material for Li-ion battery. The nanorods show good lithium ion insertion and extraction ability. It exhibits an initial specific charge and discharge capacity of 8.1 and 130.1 mAh g^{-1} , respectively, during 1.5~4.0 V at 15 mA g^{-1} . After 20 cycles, the discharge capacity of 114.3 mAh g^{-1} was maintained. The results above shows that

KV₃O₈ might have potential applications in energy devices such as electrode material for non-aqueous or aqueous Li-ion battery due to its low cost, facile synthesis, coupled with good cycling stability. However, considerable efforts should be focused on the further improvement of its discharge capacity and rate capability.

ACKNOWLEDGEMENTS

The authors greatly appreciated the financial support the National Natural Science Foundation of China (No. 20971129), Scientific Research Foundation of Central South University and The Postdoctoral Science Foundation of Central South University.

Reference

1. A.M. Morales and C.M. Lieber, *Science*, 279 (1998) 208.
2. J.M. Tarascon and M. Armand, *Nature*, 414 (2001) 359.
3. M.S. Whittingham, *Chem. Rev.*, 104 (10) (2004) 4271.
4. P.G. Bruce, B. Scrosati and J.M. Tarascon, *Angew. Chem. Int. Ed.*, 47 (2008) 2930.
5. Y. Ren, A.R. Armstrong, F. Jiao and P.G. Bruce, *J. Am. Chem. Soc.*, 132 (2010) 996.
6. J. Livage, *Materials*, 3 (2010) 4175.
7. N.A. Chernova, M. Roppolo, A.C. Dillon and M.S. Whittingham, *J. Mater. Chem.*, 19 (2009) 2526.
8. J. Jiang, Z.X. Wang and L.Q. Chen, *J. Phys. Chem.*, C 111 (2007) 10707.
9. H.M. Liu, Y.G. Wang, L. Li, K.X. Wang, E. Hosono and H.S. Zhou, *J. Mater. Chem.*, 19 (2009) 7885.
10. S. Panero, M. Pasquali and G. Pistoia, *J. Electrochem. Soc.*, 130 (1983) 1225.
11. H.M. Liu, Y.G. Wang, K.X. Wang, Y.R. Wang and H.S. Zhou, *J. Power Sources*, 192 (2009) 668.
12. G.Q. Liu, C.L. Zeng and K. Yang, *Electrochim. Acta.*, 47 (2002) 3239.
13. H.Y. Wang, K.L. Huang, S.Q. Liu, C.H. Huang, W.J. Wang and Y. Ren, *J. Power Sources*, 196 (2011) 788.
14. H.Y. Wang, S.Q. Liu, Y. Ren, W.J. Wang and A.D. Tang, *Energy&Environmental Science*, 5 (2012) 6173.
15. Y. Oka, T. Yao and N. Yamamoto, *Materials Research Bulletin*, 32 (1997)1201.
16. K. West, B. Zachau-christiansen, T. Jacobsen and S. Skaarup, *Solid State Ionics*, 40-41 (1990) 585.
17. V. Manev, A. Momchilov, A. Nassalevska, G. Pistoia and M. Pasquali, *J. Power Sources*, 43-44 (1993) 561.
18. C.C. Torardi and C.R. Miao, *Chem. Mater*, 14 (2002) 4430.
19. M.E. Spahr, P. Novák, W. Scheifele, O. Haas and R. Nesper, *J. Electrochem. Soc.*, 145 (1998) 421.
20. B. Azambre, M.J. Hudson and O. Heintz, *J. Mater. Chem.*, 13 (2003) 385.
21. L.Q. Mai, C.S. Lao, B. Hu, J. Zhou, Y.Y. Qi, W. Chen, E.D. Gu and Z.L. Wang, *J. Phys. Chem.*, B 110 (2006) 18138.
22. Y.C. Si, L.F. Jiao, H.T. Yuan, H.X. Li and Y.M. Wang, *J. Alloys Compd*, 486 (2009) 400.
23. H.Y. Wang, K.L. Huang, C.H. Huang, S.Q. Liu, Y. Ren and X.B. Huang, *J. Power Sources*, 196 (2011) 5645.
24. H. Y. Wang, K. L. Huang, Y. Ren, X. B. Huang, S. Q. Liu and W. J. Wang, *J. Power Sources*, 196 (2011) 9786.
25. H. Y. Wang, W. J. Wang, Y. Ren, K. L. Huang and S. Q. Liu, *J. Power Sources*, 199 (2012) 263.